© 2015. Published by The Company of Biologists Ltd | Journal of Cell Science (2015) 128, 1824–1834 doi:10.1242/jcs.167387

RESEARCH ARTICLE

The structure of the complex between α-tubulin, TBCE and TBCB reveals a tubulin dimer dissociation mechanism

Marina Serna[1,*], Gerardo Carranza[2,*], Jaime Martín-Benito[1], Robert Janowski[3,4], Albert Canals[3,4], Miquel Coll[3,4], Juan Carlos Zabala[2,‡] and José María Valpuesta[1,‡]

ABSTRACT

Tubulin proteostasis is regulated by a group of molecular chaperones termed tubulin cofactors (TBC). Whereas tubulin heterodimer formation is well-characterized biochemically, its dissociation pathway is not clearly understood. Here, we carried out biochemical assays to dissect the role of the human TBCE and TBCB chaperones in α-tubulin–β-tubulin dissociation. We used electron microscopy and image processing to determine the three-dimensional structure of the human TBCE, TBCB and α-tubulin (αEB) complex, which is formed upon α-tubulin–β-tubulin heterodimer dissociation by the two chaperones. Docking the atomic structures of domains of these proteins, including the TBCE UBL domain, as we determined by X-ray crystallography, allowed description of the molecular architecture of the αEB complex. We found that heterodimer dissociation is an energy-independent process that takes place through a disruption of the α-tubulin–β-tubulin interface that is caused by a steric interaction between β-tubulin and the TBCE cytoskeleton-associated protein glycine-rich (CAP-Gly) and leucine-rich repeat (LRR) domains. The protruding arrangement of chaperone ubiquitin-like (UBL) domains in the αEB complex suggests that there is a direct interaction of this complex with the proteasome, thus mediating α-tubulin degradation.

KEY WORDS: Tubulin, Protein degradation, Chaperone, Folding cofactor, Microtubule, TBCE, TBCB

INTRODUCTION

Microtubules (MTs) are essential cytoskeletal polymers that are composed of α-tubulin–β-tubulin heterodimers (tubulin dimers) that provide structural support to the cell and have important functions in key cell processes such as division, motility and intracellular transport (Kaverina and Straube, 2011). MTs are very dynamic structures that switch stochastically between growing and shrinking phases. This dynamic instability (Mitchison and Kirschner, 1984) is based on GTP binding and hydrolysis at the β-tubulin nucleotide exchangeable site (E-site). Only GTP-bound tubulin dimers can polymerize, but after polymerization the nucleotide is hydrolyzed and becomes non-exchangeable until the tubulin dimer is released from the microtubule during depolymerization (Alushin et al., 2014).

Throughout the cell cycle, the precise temporal and spatial regulation of this non-equilibrium behavior is governed largely by MT-associated proteins and by factors that control the local soluble tubulin dimer concentration accessible for MT polymerization (Lundin et al., 2010). Polymerization is regulated in part by α- and β-tubulin monomer folding and degradation, as well as by tubulin dimer formation. In contrast to actin or γ-tubulin, α- and β-tubulin require additional folding steps, which involve not only the cytosolic chaperonin complex CCT, the co-chaperone complex prefoldin (PFD) and phosducin-like proteins (PhLPs), but also Arl2 and five tubulin-binding cofactors (TBC) termed TBCA, TBCB, TBCC, TBCD and TBCE (Tian et al., 1996; Lopez-Fanarraga et al., 2001; Lundin et al., 2010). These cofactors interact differentially with α- or β-tubulin in a pathway that converges to control tubulin dimer formation (Fontalba et al., 1993; Tian et al., 1999). TBCE and TBCB are specific cofactors that interact with α-tubulin after its CCT-assisted folding (Tian et al., 1997), and TBCB has recently been shown to interact directly with CCT (Carranza et al., 2013). The TBCs are considered central factors in tubulin proteostasis because of their unique intrinsic ability to dissociate tubulin dimers (Lopez-Fanarraga et al., 2001). The tubulin dimer is very stable, with a K_d of $\sim 10^{-11}$ M, and its spontaneous dissociation is thus very unlikely (Caplow and Fee, 2002).

Overexpression of TBCE or TBCD abolishes the entire MT network of the cell, dissociating the tubulin dimer and sequestering α-and β-tubulin monomers, respectively (Martín et al., 2000; Kortazar et al., 2006; 2007). TBCB overexpression also interferes with the MT network, although less efficiently (Carranza et al., 2013). The TBCs are necessary for tubulin dimer dissociation and have an important role in regulation of MT plasticity and composition. The diversity of MT determines their dynamic properties; this is achieved by distinct tubulin isotypes leading to heterogeneity in tubulin dimer composition and by a plethora of post-translational modifications (Verhey and Gaertig, 2007). Although a large proportion of tubulin dimers might be recycled directly as new polymers, in some circumstances tubulin monomers are targeted for degradation (Lundin et al., 2010), probably through the ubiquitin-proteasome system (Mi et al., 2009).

Whereas the regulatory mechanisms of MT dynamics and tubulin biogenesis *in vitro* and *in vivo* are well described, relatively little is known about the regulation of tubulin turnover. TBCE and TBCB cooperate in tubulin dissociation both *in vivo* and *in vitro*, by sequestering α-tubulin and forming a stable ternary α-tubulin–TBCE–TBCB complex (hereafter denoted

[1]Departamento de Estructura de Macromoléculas, Centro Nacional de Biotecnología (CNB-CSIC), Madrid 28049, Spain. [2]Departamento de Biología Molecular, Facultad de Medicina, IDIVAL-Universidad de Cantabria, Santander 39011, Spain. [3]Departamento de Biología Estructural y Computacional, Institute for Research in Biomedicine (IRB-Barcelona), Barcelona 08028, Spain. [4]Departamento de Biología Estructural, Institut de Biologia Molecular de Barcelona (IBMB-CSIC), Barcelona 08028, Spain.
*These authors contributed equally to this work

‡Authors for correspondence (juan.zabala@unican.es; jmv@cnb.csic.es)

Received 10 December 2014; Accepted 16 March 2015

Journal of Cell Science (2015) 128, 1824–1834 doi:10.1242/jcs.167387

αEB) (Kortazar et al., 2007). Here, we used electron microscopy (EM) and single-particle image processing to determine the structures of human TBCE and the αEB complex, both of which are involved in α-tubulin proteostasis. We also used X-ray crystallography to determine the atomic resolution structure of the human TCBE ubiquitin-like (UBL) domain. This structure and those of homologous domains from TBCB and TBCE, as well as the α-tubulin structure, were fitted unambiguously in the EM volumes, from which we derived the molecular architecture of TBCE and the αEB complex. These model structures show the topology of TBCE and the αEB complex; in the latter, this identified the regions involved in formation of the complex, as well as putative regions that interact with the proteasome. These structural studies, combined with other biophysical techniques, biochemical assays and cell biology analyses, allow us to propose a model for the TBCE- and TBCB-mediated tubulin dissociation reaction and its implications in tubulin turnover. This study offers a new view of the α-tubulin–β-tubulin dissociation mechanism and its effects on MT dynamics and composition regulation.

RESULTS

Characterization of α-tubulin–β-tubulin dissociation by TBCE and TBCB

The post-CCT chaperones TBCE and TBCB are involved in α-tubulin folding and degradation through a poorly characterized molecular mechanism that is essential for control of cell tubulin dynamics and turnover (Lundin et al., 2010). To better understand the turnover process, we cloned, overexpressed and purified human TBCB and TBCE (Kortazar et al., 2007; Carranza et al., 2013) and analyzed their ability to dissociate tubulin dimers (Fig. 1; supplementary material Fig. S1). The α-tubulin–β-tubulin dissociation process was efficient only when both TBCE and TBCB were present in the reaction mixture; TBCB alone was unable to dissociate tubulin dimers and TBCE alone did so very inefficiently. The α-tubulin monomer released from the tubulin heterodimer was stabilized as a ternary complex with TBCE and TBCB only in the presence of both chaperones (Fig. 1; supplementary material Fig. S1A–C), whereas the β-tubulin monomer was released and became aggregated in the absence of its specific post-CCT chaperones (supplementary material Fig.

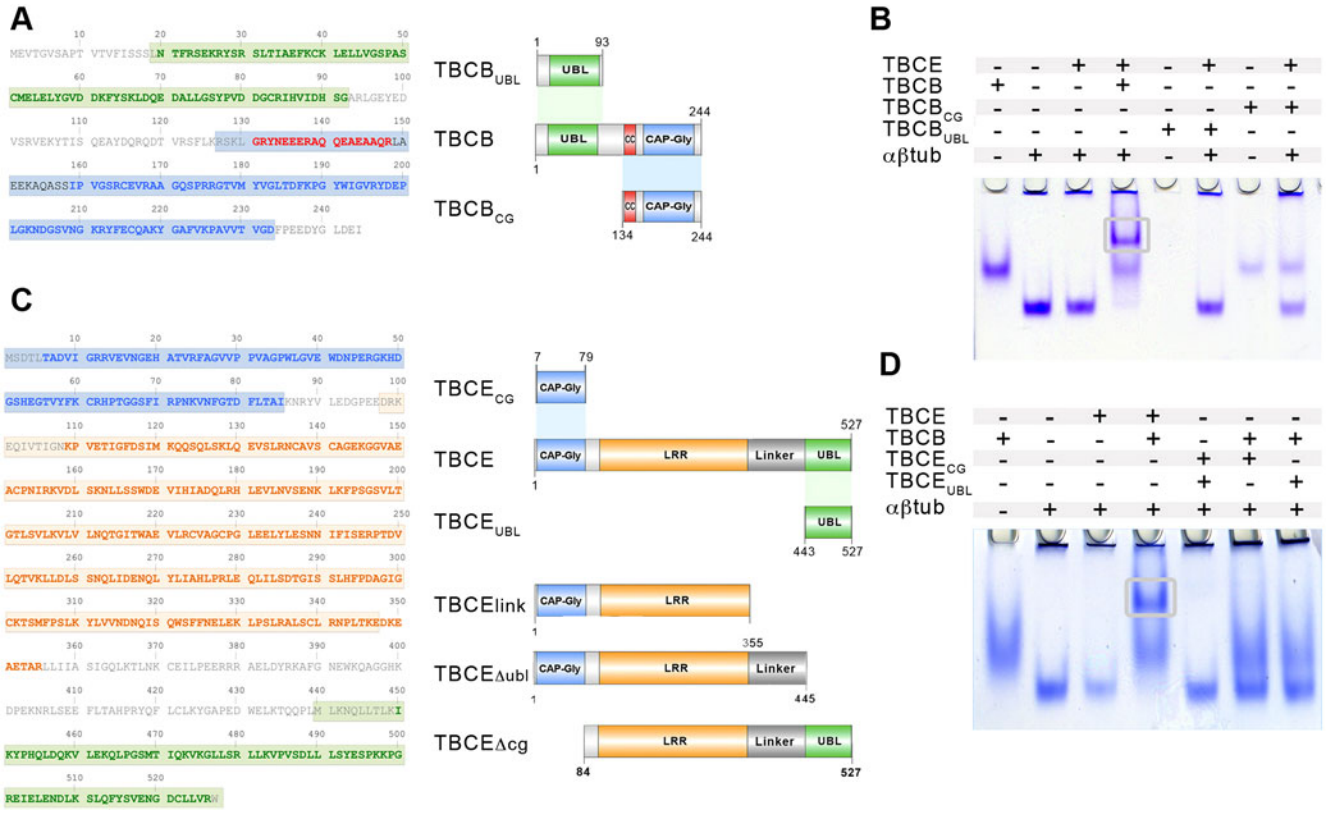

Fig. 1. α-tubulin–β-tubulin dissociation induced by TBCE, TBCB and various mutants of these two chaperones. (A) Left, amino acid sequence of TBCB; residues of the UBL (green), the coiled-coil (CC; red) and the CAP-Gly domains (blue) are highlighted. The sequences for the atomic structures of the fragments solved for this cofactor are in boxes, green for the TBCB UBL domain (PDB 1V6E) and blue for the CC and CAP-Gly domain sequences (PDB 1WHG). Right, structural domains of TBCB and the deletion mutants (TBCBubl and TBCBcg) used in the α-tubulin–β-tubulin dissociation assay. (B) α-tubulin–β-tubulin dimer dissociation analyzed by native gel electrophoresis, using TBCE and different TBCB forms (full-length, TBCBcg and TBCBubl). (C) Left, amino acid sequence of TBCE; residues of the CAP-Gly (blue), LRR (orange) and UBL domains (green) are highlighted. In the blue box, the sequence for the human UBL domain (PDB 4ICU) whose X-ray structure is reported here is shown; the orange box shows the amino acid sequence for the LRR domain from Brassinosteroid insensitive 1 from *Arabidopsis thaliana* (PDB 3RJ0), and the green box shows that for the murine TBCB CAP-Gly domain (PDB 1WHG), whose atomic structures were used for docking analyses. Right, structural domains of TBCE and the deletion mutants (TBCEcg, TBCEubl, TBCElink, TBCEΔubl and TBCEΔcg) described here. (D) α-tubulin–β-tubulin dimer dissociation analyzed by native gel electrophoresis, using TBCB and several TBCE forms (full-length, TBCEcg and TBCEubl). In the functional experiments (B,D), tubulin dimer dissociation was determined as a decrease in α-tubulin–β-tubulin band intensity as quantified by densitometry. Only full-length TBCE and TBCB generated a stable ternary complex with the two chaperones and α-tubulin (gray box).

S1D). β-tubulin aggregation was prevented when TBCA is present in the tubulin dimer dissociation assay, because this cofactor binds the β-tubulin monomer (Campo et al., 1994; Kortazar et al., 2006).

We then tested which of the TBCE and TBCB domains were involved in α-tubulin–β-tubulin dissociation. Domain organization was similar in both chaperones (Fig. 1A,C). Both proteins have a cytoskeleton-associated protein glycine-rich (CAP-Gly) and a UBL domain; in the case of TBCB, the UBL is located at the N-terminal and CAP-Gly at the C-terminal end, whereas the opposite arrangement is found in TBCE (Grynberg et al., 2003). The TBCB intermediate region has a short coiled-coil region (CC), whereas that of TBCE has a leucine-rich repeat (LRR) domain. For TBCB we cloned, expressed and purified two deletion mutants, one containing only the UBL domain (TBCBubl), and the other with the coiled-coil and CAP-Gly (TBCBcg) domains (Fig. 1A). In the case of TBCE, we used two mutants, one with only the UBL domain (TBCEubl) and the other with the CAP-Gly domain (TBCEcg) (Fig. 1C).

The α-tubulin–β-tubulin dissociation activity of the different TBCE and TBCB deletion mutants was assayed using native PAGE. Whereas full-length TBCE induced some dissociation (Fig. 1B,D), this did not occur in the presence of a TBCEubl and TBCEcg mixture (Fig. 1D). Likewise, although TBCB in the presence of full-length TBCE induced tubulin dimer dissociation there was no dissociation when TBCB was combined with TBCEubl or TBCEcg (Fig. 1D). These experiments show that there is efficient tubulin dissociation in the presence of the two chaperones, and that whereas the TBCE LRR domain is important in this process, the TBCB UBL domain is dispensable (Fig. 1B,D).

Structure of TBCE and the αEB complex

To analyze the TBCE structure, we used negative staining EM, a technique suitable for small specimens such as TBCE (~60 kDa). A total of 12,000 particles were selected and used to generate a 3D reconstruction (Fig. 2A; supplementary material Fig. S2; 18 Å resolution). The refined structure showed an asymmetric, L-shaped volume with one short globular arm and a long, flat arm from which a small globular domain protrudes.

The ternary αEB complex was generated by incubating TBCE and TBCB with tubulin dimers and purifying the stable complex by size exclusion chromatography (supplementary material Fig. S1D) (Kortazar et al., 2007). Owing to the small size of the complex (~140 kDa), it was also prepared for negative staining EM. We selected 26,129 particles, which were used to generate a 3D reconstruction of the αEB complex (Fig. 2B; supplementary material Fig. S2, 21 Å resolution). This structure is U-shaped, with two curved arms composed of small, globular domains placed almost symmetrically relative to a larger, globular base. For both TBCE and αEB, parallel and independent reconstructions from different initial models were carried out to validate the final model.

Topology of the αEB complex

We then determined the positions of TBCE, TBCB and α-tubulin within αEB. We deduced the location of TBCE directly, by comparing the refined 3D structures of TBCE and αEB (Fig. 2C); this showed that the TBCE structure and conformation were almost completely conserved in αEB. To ascertain TBCB position and orientation in the complex, we designed and purified an N-terminal GFP-tagged human TBCB fusion protein (TBCB–GFP). The tubulin dimer dissociation activity of TBCB–GFP was similar to that of wild-type TBCB, and it maintained its ability to form a stable ternary complex with α-tubulin and TBCE (αEB–GFP) (Fig. 3A). This αEB–GFP complex was purified by gel filtration chromatography (Fig. 3B) and analyzed by EM to generate the final volume using 16,702 selected particles (Fig. 3C; supplementary material Fig. S2, 23 Å resolution). The 3D structure of the αEB–GFP complex showed features very similar to those of αEB, with the exception of an extra mass protruding from the end of one arm (compare Fig. 3C and Fig. 3E). This extra density fits accurately with the GFP size and barrel-shaped structure (Fig. 3D), which allowed us to assign the TBCB position unambiguously in this arm of the αEB complex, whose dimensions (~60×30 Å) are compatible with TBCB

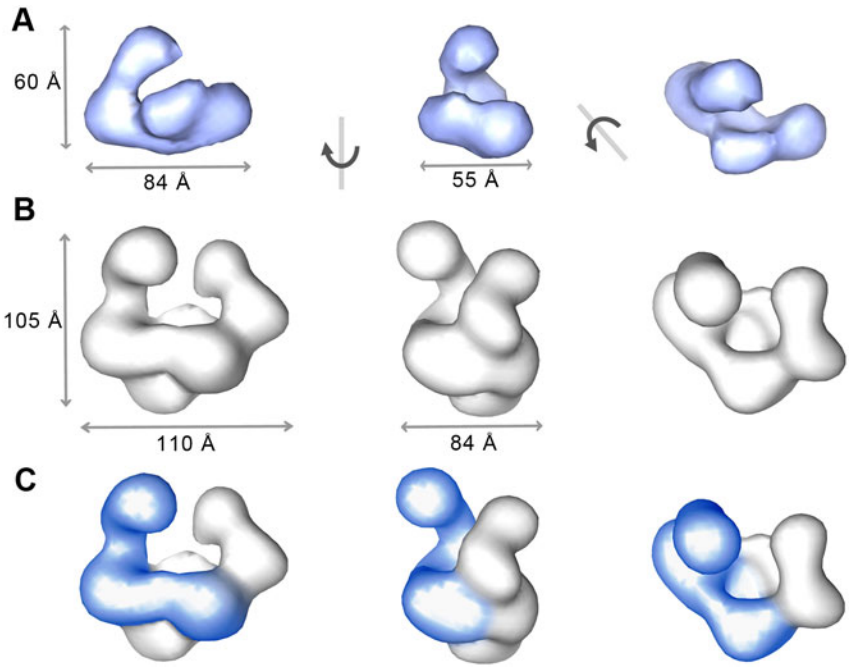

Fig. 2. 3D structure of TBCE and the αEB complex. Series of orthogonal views and dimensions are shown. (A) 3D reconstruction of TBCE. (B) 3D reconstruction of the αEB complex. (C) Localization of the TBCE density map (blue) within the αEB complex.

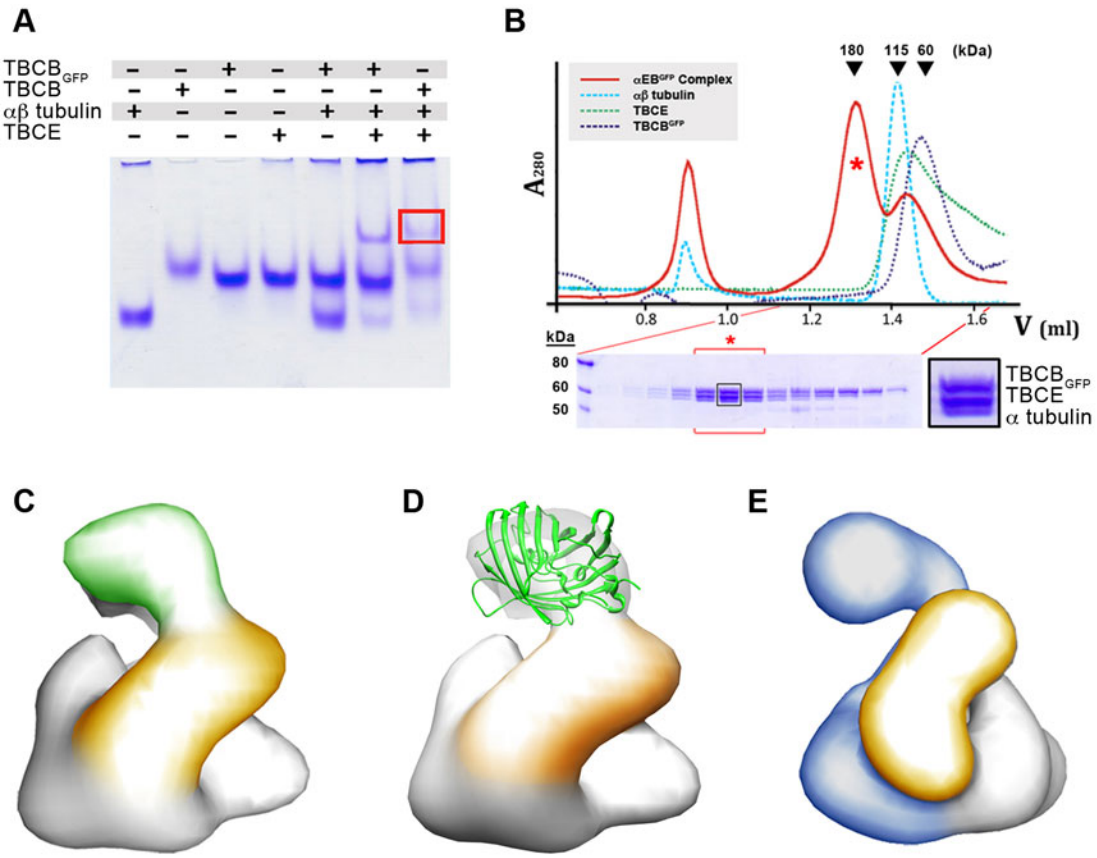

Fig. 3. Purification and 3D structure of the ternary αEB–GFP complex. (A) The TBCB–GFP mutant retains its ability to enhance tubulin dissociation by TBCE. The presence of the fusion protein in the reaction substantially reduces the amount of the tubulin dimer with respect to the control with TBCE alone as it is shown in the Coomassie-stained native gel. The presence of both TBCE and TBCBgfp cofactors leads to the formation of an αEB–GFP complex (highlighted with a red box) with an electrophoretic mobility similar to the αEB complex. (B) Gel filtration chromatography purification of the ternary αEB–GFP complex (red profile). A high-molecular-mass peak that contains the complex (indicated with an asterisk) is separated from TBCE, TBCB and tubulin dimers, whose mobility controls are depicted as discontinuous green, dark blue and light blue, respectively. (C) Side view of the 3D reconstruction of the αEB–GFP complex, where the green density belongs to GFP and the yellow one to TBCB. (D) The same view of αEB–GFP complex with the atomic structure of GFP fitted within the assigned density. (E) The same view of the αEB complex, in which the TBCE density is colored blue and TBCB, yellow.

molecular mass (~27 kDa). These results imply that the TBCB CAP-Gly domain is in close contact with the main body of the complex, whereas the UBL domain protrudes from the structure. This latter result is consistent with the finding that this domain did not alter dissociation activity (Fig. 1B), and confirmed the TBCB orientation suggested by 3D reconstruction. The remainder of the αEB density not occupied by TBCE or TBCB and represented by the large central core would correspond to α-tubulin; the dimensions and shape of this region are compatible with those of an α-tubulin molecule.

The TBCE CAP-Gly domain interacts specifically with the α-tubulin C-terminal EEY motif

The CAP-Gly domain is a sequence of 80 amino acids, conserved from yeast to man, that is typically defined as a tubulin-interacting domain. One of its main structural and functional features is a conserved GK(N/H)DG motif that defines a basic groove. In some proteins like CLIP170 (also known as CLIP1) or the p150^{Glued} (also known as DCTN1) subunit of the dynactin 1 complex, this basic groove is involved specifically in binding the EEY motif in the acidic C-terminal tail of several proteins such as α-tubulin or EB1 (Steinmetz and Akhmanova, 2008).

The TBCE N-terminal CAP-Gly domain is crucial for the α-tubulin interaction during tubulin folding and dissociation reactions. Characterization of this interaction could help to define the correct position of each domain within TBCE structure and thus, within the αEB complex. We first subjected tubulin dimers to limited proteolysis with the serine endopeptidase subtilisin to generate C-terminus-truncated forms (α-S-tubulin and β-S-tubulin), which were further purified by gel filtration chromatography; dimers were then dissociated by adding TBCE or TBCE plus TBCB. Native gel electrophoresis and western blot experiments showed a complete lack of cofactor-dissociating activity (Fig. 4A).

We analyzed the role of the tyrosine residue in the α-tubulin EEY C-terminal motif by treatment with carboxypeptidase A (CPA), an exopeptidase that specifically removes aromatic residues at the C-terminal end of a target protein. After detyrosination of the tubulin dimers (ΔYtubulin), confirmed by western blot analysis with anti-tyrosinated tubulin antibody, dimers were purified by gel filtration chromatography. The modified dimers were incubated with TBCE and analyzed by native gel electrophoresis, which showed that this cofactor was unable to dissociate the ΔYtubulin dimer (Fig. 4B).

Journal of Cell Science (2015) 128, 1824–1834 doi:10.1242/jcs.167387

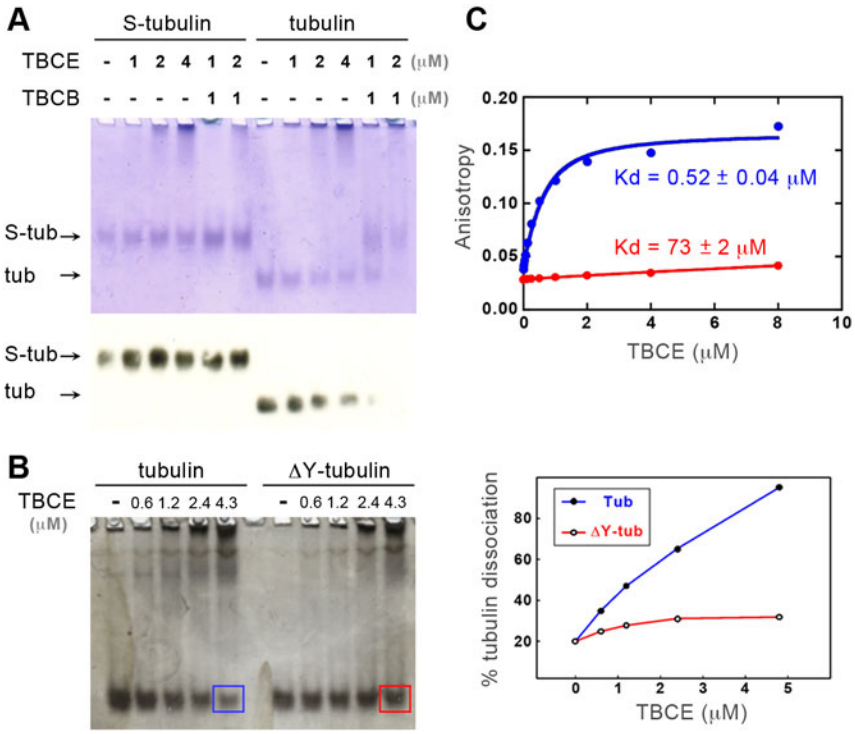

Fig. 4. The α-tubulin C-terminal EEY motif binds specifically to TBCE. (A) TBCE alone is able to dissociate wild-type but not S-tubulin dimers, as monitored by reduction in the amount of tubulin dimer in a Coomassie-stained native gel. The lower panel shows a western blot analysis using anti-β-tubulin antibody. (B) Incubation of TBCE with wild-type or ΔY-tubulin dimers leads to dimer dissociation only with wild-type tubulin. Right, TBCE dissociative activity with wild-type (blue line) or ΔY-tubulin dimers (red line). (C) Fluorescence anisotropy curves obtained after incubation of increasing concentrations of TBCE with two fluorescein-tagged peptides, one with the ten last residues of the α-tubulin acidic tail (blue) and one without the final tyrosine residue (red). K_d values expressed as mean±s.d.

To analyze the EEY motif interaction with the TBCE CAP-Gly domain by fluorescence anisotropy, we designed two fluorescein-tagged peptides, one with the last ten residues of the acidic tail of α-tubulin isotypes 1 and 2 (GEGEEEGEEY), and the other without the last tyrosine residue (GEGEEEGEE). The two peptides were incubated with increasing TBCE concentrations, and fluorescence intensity was measured to calculate the dissociation constant for each. The tubulin peptide lacking the final residue showed a greatly reduced affinity (140 times less) for the TBCE CAP-Gly domain compared to the longer peptide (dissociation constant 73 µM compared to 0.53 µM; Fig. 4C). This finding confirms the need for this amino acid for efficient TBCE interaction and tubulin dimer dissociation.

Structure of the human TBCE UBL domain

Although crystallization of the full-length TBCE and TBCB was unsuccessful, probably due to their intrinsic flexibility, we determined the crystal structure of the human TBCE UBL domain (Q444-W527) at 1.45 Å resolution (supplementary material Table S1) by single-wavelength anomalous diffraction (SAD), using a praseodinium (III) heavy-atom derivative. The UBL structure consists of a five-stranded, mixed β-sheet of topology 21534 that diagonally cradles an α-helix at its concave face (Fig. 5A). This β-grasp fold is characteristic of ubiquitin and UBL domains in many proteins. A structural comparison of human TBCE UBL and ubiquitin (PDB code 1TBE; Cook et al., 1994) confirms the similarity of these protein structures (r.m.s.d. 1.4 Å for 72 equivalent Cα atoms), although sequence identity is low (20%) (Fig. 5B,C). The main differences are related to the length and the conformation of two loops, L1 (that connects strands S1 and S2) and L4 (that connects strands S3 and S4), which define a deep groove at the face of the β-sheet that is opposite to the one holding the α-helix (Fig. 5D). The equivalent groove in ubiquitin participates in the interaction with the

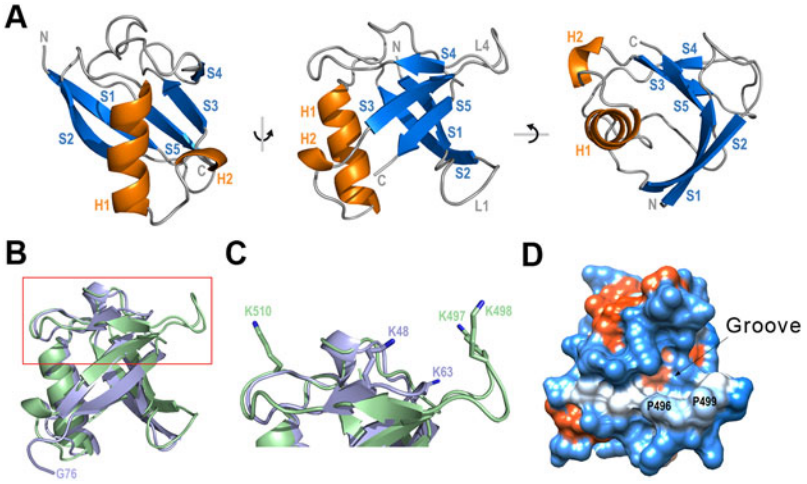

Fig. 5. Crystal structure of the human TBCE UBL domain. (A) Three orthogonal views of the structure. The α-helices H1 and 3_{10} H2 are depicted in orange, β-strands (S1–S5) in blue, and loops and connecting regions in gray (only loops L1 and L4 are labeled). (B) Superposition of the UBL domain of TBCE (green) and ubiquitin (pale blue; PDB 1TBE). Ubiquitin C-terminal residue G76, essential for polyubiquitylation, is labeled for reference. (C) Close-up of the area indicated by a red rectangle in B, showing the lysine side chains for both structures. (D) Electrostatic surface of the TBCE UBL domain showing the hydrophobic patch (white) extending from the lower part of the groove. Proline residues 496 and 499 are labeled for reference.

ubiquitin-interacting motif (UIM) of the proteasome subunit Rpn10 (Riedinger et al., 2010).

Human TBCE UBL has no lysine residues at positions equivalent to ubiquitin K48 and K63, the sites for poly-ubiquitin linkage, although there are three exposed lysine residues, K497 and K498 at loop L4, and K510 at loop L5 (Fig. 5C). The C-terminal part is five residues shorter in human TBCE UBL and does not have the tandem glycine residues that in ubiquitin are responsible for covalent bond formation with target protein lysine residues (ubiquitylation) or ubiquitin polymerization.

Molecular architecture of the αEB complex

After localizing TBCE, TBCB and α-tubulin within αEB and determining the interacting regions between TBCE and α-tubulin, we docked the atomic structures of the TBCB (CAP-Gly and UBL), TBCE (CAP-Gly, LRR and UBL) and α-tubulin domains into the 3D reconstruction of the αEB complex (supplementary material Movie 1). As there is no information for the atomic structure of human TBCE and TBCB domains except the TBCE UBL domain (Fig. 5), we used the atomic structures of homologous proteins to dock the remainder of the protein domains.

Docking of the two TBCB domains was straightforward, given that comparison of the 3D reconstructions of αEB and αEB–GFP located the TBCE UBL domain at the tip of one arm of the complex (Fig. 3C–E). The nuclear magnetic resonance (NMR) structures of the murine UBL and CAP-Gly domains [PDB codes 1V6E (Lytle et al., 2004) and 1WHG; 82% and 83% sequence identity with the human counterparts, respectively; supplementary material Fig. S3A,B] were docked such that the former was located at the tip and the latter at the base of the small globular domain (Fig. 6A).

The functional domains of TBCE were also docked into the αEB complex. For the LRR domain, we used the atomic structure of the closest structural homolog, the LRR domain of the kinase Brassinosteroid insensitive 1 (BRI1) in *Arabidopsis thaliana* (80.2% sequence identity) (PDB code 3RJ0; Hothorn et al., 2011) (supplementary material Fig. S3C). Owing to its solenoid shape, this structure fits unambiguously into the concave central region in both the αEB complex (Fig. 6B) and TBCE (Fig. 6D).

This leaves the localization of the other two domains, UBL and CAP-Gly, at the ends of the LRR domain. The CAP-Gly domain was assigned by considering the following points. First, that the conserved GKHDG motif, present in the CAP-Gly domain, must be in contact with the density of α-tubulin, as shown previously (Fig. 6B). Second, that TBCE and TBCB have recently been shown to form a transient complex before tubulin dimer dissociation – this interaction is mediated by the last three residues of the TBCB C-terminal domain (DEI), similar to the α-tubulin C-terminal EEY motif (Carranza et al., 2013), and the TBCB and TBCE CAP-Gly domains must therefore make contact. Finally, that the TBCBcg mutant assists tubulin dimer dissociation mediated by TBCE (Fig. 1B), again suggesting that both CAP-Gly domains are in proximity.

Our tubulin dimer dissociation experiments showed that both TBCE and TBCB are needed for 100% dissociation of tubulin in a stoichiometric reaction, whereas no dissociation takes place when only TBCB is present, and only ~35% dissociation occurs in the presence of TBCE alone. The available atomic structures of TBCE domains occupied most of the density ascribed to this protein within the ternary complex. The exception was a region between the UBL and LRR domains (hereafter, the linker; ~100 residues,

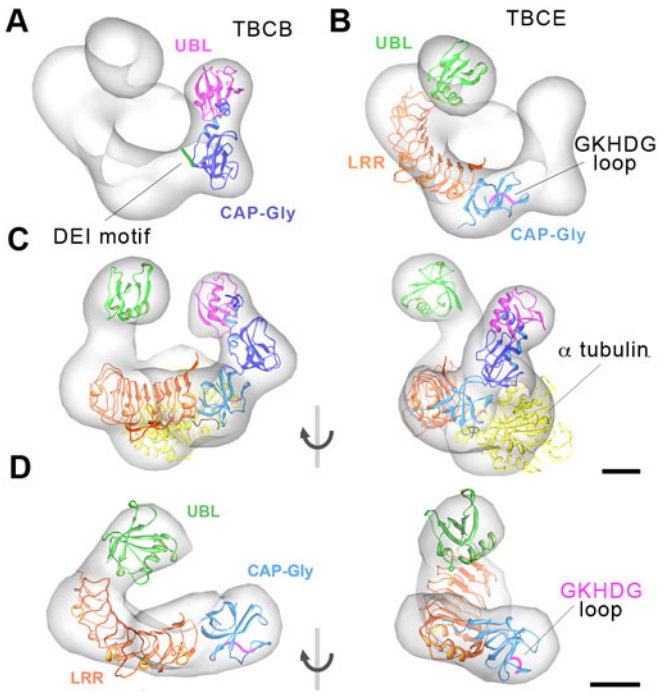

Fig. 6. Molecular architecture of TBCE and the αEB complex. (A) Docking of the TBCB UBL domain (magenta; PDB 1V6E) and CAP-Gly domain (dark blue; PDB 1WHG). The TBCB acidic C-terminal tail (DEI), involved in the interaction with TBCE, is in green. (B) Docking of the solved atomic structure of the human TBCE UBL domain (green; PDB 4ICU and 4ICV), the LRR domain (orange; PDB 3RJ0), and the CAP-Gly domain (light blue; PDB 1WHG), within the density assigned to TBCE. The conserved CAP-Gly domain GKHDG motif, involved in the interaction with the α-tubulin C terminus, is highlighted in magenta. (C) Two orthogonal views showing all domain structures fitted into the αEB ternary complex, including α-tubulin (yellow; PDB 1TUB). (D) The same views of the 3D reconstruction of TBCE with fitting of the domain structures. Scale bars: 2 nm.

Fig. 1C), whose structure has not yet been determined, but which is involved in α-tubulin–β-tubulin dissociation. Addition of the TBCBubl mutant to TBCE did not increase tubulin dimer dissociation, whereas TBCBcg increased dissociation (Fig. 1B). Given these findings, the TBCE CAP-Gly domain must make contact with its TBCB counterpart; indeed, the docking of a CAP-Gly domain between the TBCE LRR domain and the TBCB CAP-Gly domain showed a good fit (Fig. 6B,C).

Once the CAP-Gly and LRR domains were placed, the TBCE UBL domain was located to the other small globular domain of the part assigned to this cofactor in the αEB complex. Docking of our human atomic structure into this globular domain was also good, not only in the αEB complex (Fig. 6B), but also in the TBCE structure (Fig. 6D). Finally, the atomic structure of α-tubulin (Nogales et al., 1998) was docked into the globular domain at the base of the αEB structure (Fig. 6C). The best docking left the α-tubulin C-terminal region facing the TBCE CAP-Gly domain; this docking was reinforced by the biochemical findings showing specific interaction between the C-terminal region of the cytoskeletal protein and the TBCE CAP-Gly domain (Fig. 4).

In vivo analysis of tubulin dissociation activity of truncated TBCE mutants

The proposed molecular architecture of αEB indicates that the closest contacts TBCE establishes with α-tubulin take place at

Journal of Cell Science (2015) 128, 1824–1834 doi:10.1242/jcs.167387

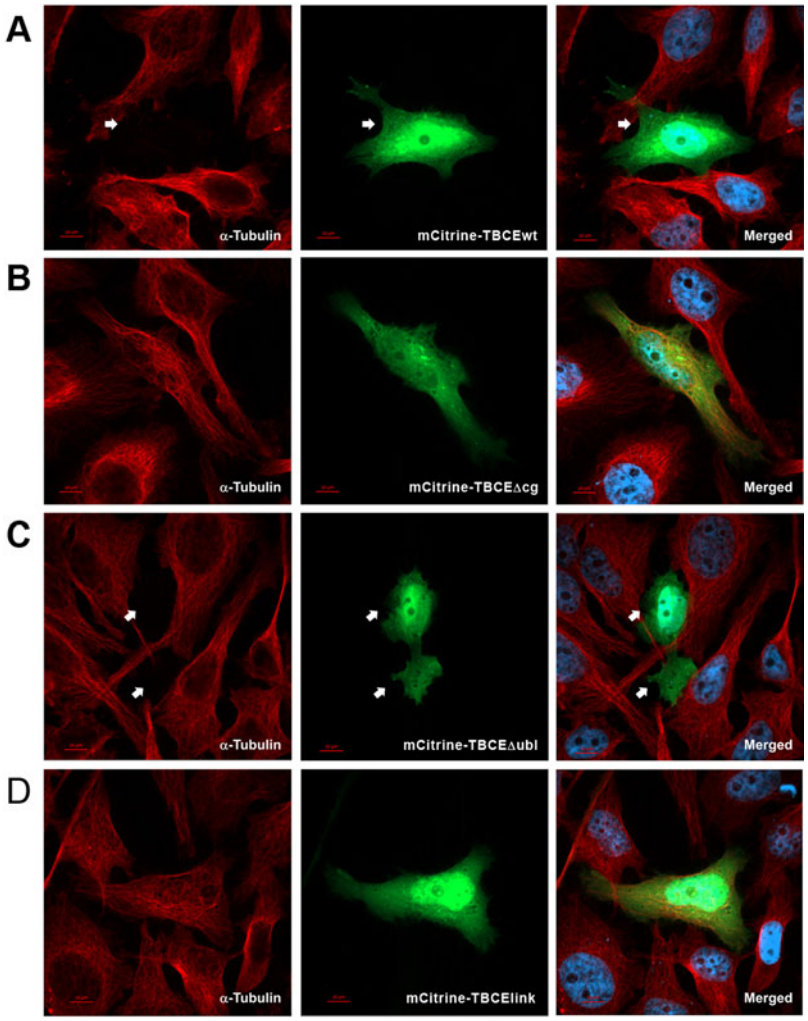

Fig. 7. *In vivo* microtubule depolymerization activity is abolished in truncated TBCEΔcg and TBCElink mutants. Confocal microscopy images of HeLa cells overexpressing (A) wild-type TBCE, (B) TBCEΔcg, (C) TBCEΔubl and (D) TBCElink mutants. α-tubulin (red, left column) and the overexpressed TBCE mutants (green, center) are shown. Nuclei (blue) were stained with Hoechst 33258 in the merged images (right). White arrows indicate cells that completely lack a microtubule network when wild-type TBCE or TBCEΔubl was overexpressed.

both ends of the central cavity and include its CAP-Gly and LRR domains, as well as the linker that connects the UBL domain. We reasoned that this tight association might be central to the tubulin dissociation reaction. To confirm this hypothesis, we designed three TBCE deletion mutants that lack the UBL domain (TBCEΔubl), the UBL domain and the linker (TBCElink), or the CAP-Gly domain (TBCEΔcg) (Fig. 1C). Each truncated TBCE mutant was cloned as a citrine fusion protein and used to transfect HeLa cells (Fig. 7). Confocal microscopy images of HeLa cells in which these TBCE mutants were overexpressed clearly indicated that absence of the UBL domain did not affect TBCE MT depolymerization activity (Fig. 7C), whereas this activity was abolished in the absence of the CAP-Gly domain (Fig. 7B) or the linker (Fig. 7D). These findings confirm the importance of these two regions and the central LRR domain in the tubulin dimer dissociation process, as well as the irrelevance of the UBL domain, and are thus consistent with our model.

GTP hydrolysis is not necessary for tubulin dimer dissociation

TBCE and TBCB are able to dissociate tubulin dimers with GTP at the non-exchangeable site and GDP or GTP at the exchangeable site (E-site, Jacobs, 1975; Kortazar et al., 2007). It was thus possible that these cofactors mediate tubulin dissociation through hydrolysis of GTP bound to the α-tubulin subunit. To resolve this issue, and given that in our *in vitro* system this GTP bound to α-tubulin is the only external source of energy available for tubulin dissociation, we developed an assay that allowed accurate measurement of GTP and GDP amounts before and after tubulin dissociation. Tubulin dimers were subjected to an assembly–disassembly cycle to produce tubulin dimers containing mostly GDP at the E-site. After purification, the GDP–tubulin dimers were completely dissociated in the presence of over-stoichiometric amounts of TBCE and TBCB. GTP and GDP were then isolated and quantified by HPLC (supplementary material Fig. S4). We found the same GTP:GDP ratio before and after tubulin dissociation, which shows that GTP hydrolysis is unnecessary for tubulin dimer dissociation by TBCE and TBCB, and therefore that no energy is needed in the dissociation process. The tubulin dimer is a very stable complex with a K_d of 10^{-11} M (Caplow and Fee, 2002). The absence of energy consumption during its dissociation points to the importance of TBCE and TBCB activity, which give rise to a very stable αEB complex. It is tempting to suggest that, after TBCE and TBCB interaction with the tubulin dimer, an unstable, quaternary α-tubulin–β-tubulin–TBCE–TBCB (αβEB) complex is formed that could have greater free energy, which would in turn drive the reaction to the final αEB complex. To date, no intermediate αβEB complex has been isolated or reported.

DISCUSSION

One of the central questions in MT dynamic regulation is the control of local free tubulin dimer concentration, which in turn depends on tubulin dimer formation and dissociation. TBCs are implicated in these processes (Tian et al., 1996); TBCE and TBCB control the α-tubulin biogenesis and degradation pathways. The scarcity of structural information regarding these TBCs has nonetheless prevented elucidation of the molecular mechanisms of these functions.

Our functional assays with various TBCE and TBCB mutants, together with the EM structural determination of TBCE and the αEB complex, and interpretation by molecular fitting of the protein domain atomic structures, allowed us to develop a model that explains the molecular mechanism by which tubulin cofactors cooperate in dimer dissociation and guide the α-tubulin monomer towards degradation. 3D reconstruction of TBCE showed an L-shaped structure with its central core domain occupied by a large concave LRR domain, whereas the two other functional domains, CAP-Gly and UBL, occupy two globular regions at either side of the central domain (Fig. 6D).

Based on the literature and our own observations, TBCE alone is able to dissociate the tubulin dimer *in vitro* (Kortazar et al., 2007), which indicates direct interaction with α-tubulin. There is nonetheless no biochemical or structural evidence that could help map this interaction. Only one previous structure prediction study proposed that TBCE has an N-terminal CAP-Gly domain, typically involved in tubulin binding, which could be responsible for such an interaction (Grynberg et al., 2003). The CAP-Gly domains have a conserved basic groove composed of the GK(N/H)DG consensus motif, which specifically binds the conserved EEY motif at the end of the α-tubulin acidic C-terminal tail (Steinmetz and Akhmanova, 2008). Here, we show that the EEY motif is involved in TBCE interaction, as TBCE tubulin dimer dissociation activity is impaired when the last aromatic residue in the motif is absent (Fig. 4, Fig. 8A). This interaction could also be responsible for TBCE specificity for α-tubulin, given that β-tubulin lacks this C-terminal motif. We clearly established the *in vivo* role of the TBCE CAP-Gly domain in tubulin dimer dissociation, as MTs did not depolymerize in cells transfected with a TBCE mutant that lacked this domain (Fig. 7C).

Our analysis of the molecular architecture of αEB suggests that TBCE establishes additional interactions with α-tubulin, specifically between helix H12 of the cytoskeletal protein and the region that comprises the LRR domain and the linker. This was confirmed by our finding that MTs did not depolymerize in the presence of the isolated TBCE CAP-Gly domain or in experiments in which the linker was absent (Fig. 7D). The additional interaction surfaces provided by the LRR and the linker might be essential not only for dissociation but also for α-tubulin monomer stabilization, given that isolated monomeric tubulin forms aggregates (Lopez-Fanarraga et al., 2001; Kortazar et al., 2007). Whereas TBCE interacts with and dissociates the tubulin dimer, a stable complex is formed between this cofactor and α-tubulin only when TBCB is present (Kortazar et al., 2007). Although previous studies have suggested that there is an association between TBCB and TBCE (Grynberg et al., 2003; Kortazar et al., 2007), the only direct physical interaction characterized to date is between TBCE and the acidic TBCB C-terminal tail (Carranza et al., 2013). Analysis of the molecular architecture of the αEB complex suggests that TBCB interacts with TBCE, whereas there appears to be no notable interaction between TBCB and α-tubulin in the ternary complex. Indeed, as human TBCB is reported not to interact with native tubulin dimers (Tian et al., 1997; Kortazar et al., 2007), involvement of this cofactor in the α-tubulin dissociation pathway appears to be through interaction with and regulation of TBCE activity.

Based on our model, placement of the TBCE CAP-Gly domain with the GKHDG motif orientated towards the C-terminal end of

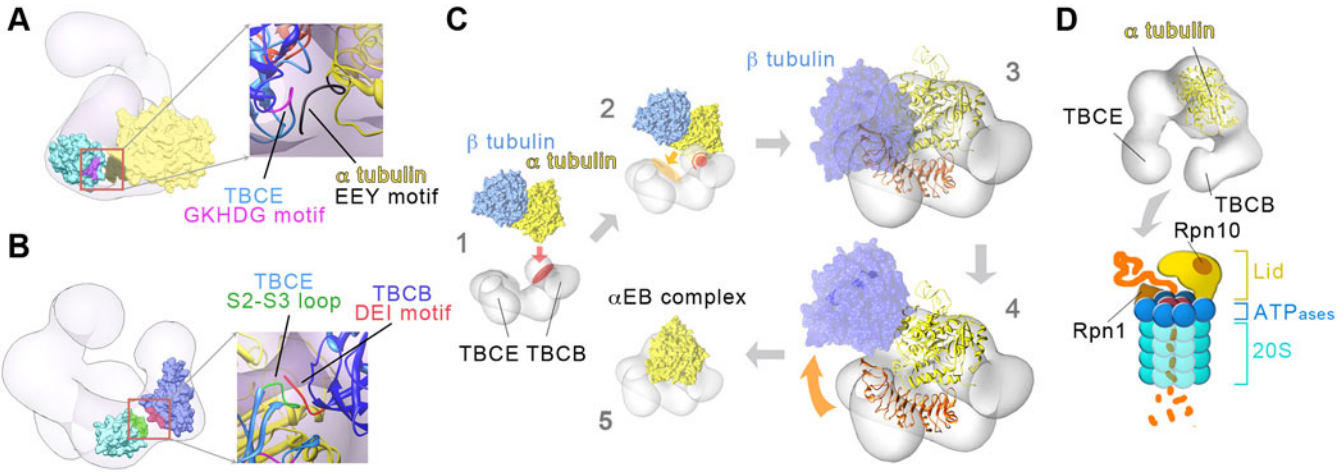

Fig. 8. Proposed model for the dissociation of tubulin dimers by the EB complex and its possible effect in tubulin degradation. (A) Interaction between the docked TBCE CAP-Gly domain (light blue) and α-tubulin (yellow); the right image shows an enlargement of the contact regions, comprised of the TBCE CAP-Gly domain GKHDG motif (magenta) and the α-tubulin EEY motif (black). (B) Interaction between TBCE CAP-Gly domain (light blue) and the TBCB acidic tail next to its CAP-Gly domain (dark blue). A magnified view of the atomic structure of TBCE CAP-Gly (light blue) including the conserved S2–S3 loop (green) that might be responsible for interaction with the DEI motif in the TBCB acidic tail (red) is shown on the right. (C) Model of the TBCE- and TBCB-assisted tubulin dimer dissociation mechanism. (1) A binary TBCE:TBCB complex interacts with α-tubulin in the dimer through the TBCE CAP-Gly domain GKHDG motif (red). (2) Next, α-tubulin establishes additional contacts with the TBCE LRR domain and linker (orange), producing (3) a steric impediment between the LRR domain and β-tubulin (light blue) that (4) forces release of the latter, and (5) leads to formation of a stable αEB complex. (D) The ternary αEB complex might guide α-tubulin to the proteasome. The UBL domains of the tubulin cofactors would interact specifically with the Rpn1 and/or Rpn10 proteasomal subunits.

α-tubulin (Fig. 8A) leaves the S2–S3 loop of this domain to be positioned near the DEI motif of the TBCB acidic C-terminal tail. A similar arrangement was described for interaction of the CAP-Gly domains of $p150^{Glued}$, tubulin and EB1, where the basic groove of $p150^{Glued}$ contacts the α-tubulin acidic tail and the S2–S3 loop interacts specifically with EB1 (Steinmetz and Akhmanova, 2008) (Fig. 8B). In summary, the TBCE CAP-Gly domain appears to have a crucial role in tubulin dimer dissociation and subsequent α-tubulin stabilization by binding TBCB and α-tubulin.

TBCE is able to dissociate the tubulin dimer *in vitro* without the assistance of any other cofactor, but TBCB clearly enhances this activity (Kortazar et al., 2007; Carranza et al., 2013; this study). Given that TBCE retains its dissociative ability alone, this must be regulated through activity enhancement, probably based on a conformational change in TBCE after TBCB interaction. This change would affect the TBCE CAP-Gly domain, increasing its accessibility to α-tubulin. The resolution of the 3D reconstructions of TBCE and the αEB complex is insufficient to confirm this conformational change.

The molecular architecture of the αEB complex helps to clarify the molecular mechanism of TBCE- and TBCB-mediated tubulin dimer dissociation (Fig. 8C). Although TBCC is the only tubulin cofactor whose catalytic activity has been reported (Tian et al., 1999), we tested whether energy from possible GTP hydrolysis in α-tubulin could be used for tubulin dimer dissociation. We measured the amounts of GTP and GDP in the reaction before and after tubulin dissociation and found no significant differences; this implies that the TBCE- and TBCB-mediated tubulin dimer dissociation reaction is independent of energy (supplementary material Fig. S4).

As to how heterodimer dissociation takes place, the answer appears to lie in the position of the β-tubulin molecule. Fitting the heterodimer into the αEB complex using the α-tubulin position in our model as a template reveals a steric impediment between β-tubulin and the TBCE linker. We demonstrated the importance not only of the TBCE CAP-Gly domain in dissociating tubulin dimers (Fig. 4; Fig. 7B) but also that of the linker, given that its absence impairs this activity (Fig. 7D). It is tempting to suggest a model whereby tubulin dimer dissociation is assisted by TBCE and TBCB (Fig. 8C; supplementary material Movie 1) as follows. First, tubulin dimers are first recognized and bound by the TBCE CAP-Gly domain. This process would be enhanced by formation of a TBCE–TBCB binary complex (Carranza et al., 2013), generated by interaction of the TBCE CAP-Gly domain and the TBCB acidic tail. Second, the α-tubulin monomer then establishes a number of additional interactions with the LRR domain of TBCE, such that the C-terminal end of the LRR domain and the linker contact the β-tubulin monomer. Third, as a result of this interaction, an induced conformational change in the heterodimer would destabilize the α-tubulin–β-tubulin interface, resulting in β-tubulin monomer release and finally generation of the final, stable αEB complex.

The tubulin degradation pathway contributes to the proteostasis of these cytoskeletal proteins. Although it has never been thoroughly investigated, recent studies have indicated that this degradation process is relevant to human diseases (Lundin et al., 2010). Tubulin is degraded by the ubiquitin-proteasome system (Mi et al., 2009) through an unknown mechanism that might involve some of the TBCs (Bartolini et al., 2005; Keller and Lauring, 2005; Lundin et al., 2010). The UBL domains are typically involved in proteasome-mediated proteolysis through specific interaction with the Rpn10 subunit of the proteasome, through transfer of ubiquitylated substrates to the proteolytic machinery and/or formation of ubiquitin–protein conjugates (Upadhya and Hegde, 2003). Pac2, the TBCE ortholog in budding yeast, also interacts through its UBL domain with the proteasome Rpn10 subunit, to mediate Pac2 turnover (Voloshin et al., 2010). In the αEB complex structure shown here, the UBL domains of both TBCE and TBCB cofactors remain free and accessible for the proteasome interaction needed for α-tubulin degradation. The groove in the TBCE UBL domain, which in ubiquitin docks with the Rpn10 UIM α-helix (Riedinger et al., 2010), is fully accessible and points towards the tip of one of the protruding lobules of the complex (Fig. 8D). In TBCEubl, this groove contains an elongated hydrophobic patch on one wall that might be appropriate for protein–protein interaction (Fig. 5D). Whereas TBCE and TBCB, both of which have a single UBL domain, can interact on their own with the isolated α-tubulin monomer in the heterodimer formation pathway (Tian et al., 1997), TBCB cannot interact on its own with the tubulin dimer (Carranza et al., 2013). The simultaneous presence of both UBL domains in the αEB complex could thus be a signal for tubulin heterodimer disassembly and would drive the α-tubulin monomer towards proteasomal degradation (Fig. 8D). This mechanism would resemble the classical cooperation of a UBL domain with its closely related homolog, the ubiquitin-associated (UBA) domain, which act as a carrier to deliver ubiquitylated substrates to the proteasome (Kaplun et al., 2005).

In summary, we have determined, by performing EM, the structure of the human αEB complex formed after α-tubulin–β-tubulin dissociation assisted by chaperones TBCE and TBCB. We have found the dissociation process is energy-independent and takes place through a disruption of the α-tubulin–β-tubulin interface that is caused by a steric interaction between β-tubulin and the TBCE CAP-Gly, LRR and linker domains. The protruding arrangement of the two UBL domains in the αEB complex points to a direct interaction of this complex with the proteasome, thus mediating α-tubulin degradation. This study offers a new view of the α-tubulin–β-tubulin dissociation mechanism and its consequences on MT dynamics.

MATERIALS AND METHODS

Protein production

Human TBCE and TBCB were cloned and purified from insect cells infected with recombinant baculovirus and *Escherichia coli* cells, respectively (Kortazar et al., 2007). Tubulin dimers were purified from bovine brain (Avila et al., 2008). The TBCB–GFP fusion protein was expressed in BL21(DE3)pLysS *E. coli* cells and purified by hydrophobic (phenyl-Sepharose column, GE-Healthcare) and ion exchange (HiTrapQ HP and MonoQ 4.6/100 PE columns, GE-Healthcare) chromatography. TBCBubl and TBCBcg were also expressed in BL21(DE3)pLysS *E. coli* cells and purified by affinity chromatography (HisTrap HP, GE-Healthcare). TBCB–GFP, TBCBubl and TBCBcg were further purified by gel filtration chromatography (Superdex 75 10/300 GL column, GE-Healthcare). TBCEubl was expressed in B834(DE3) *E. coli* cells and purified by affinity (HisTrap HP, GE-Healthcare) and gel filtration (Superdex 75 HL 16/60 column, GE-Healthcare) chromatography. TBCEΔcg, TBCEΔubl, and TBCElink mutants were cloned into the pSI-DAL2 plasmid for expression in mammalian cells. The primers used in the cloning of the TBCE and TBCB mutants are shown in supplementary material Table S2.

Tubulin dimer dissociation activity assay and purification of αEB and αEB–GFP protein complexes

Activity was assayed for each tubulin cofactor by analyzing tubulin heterodimer dissociation ability by non-denaturing gel electrophoresis

(Zabala and Cowan, 1992; Kortazar et al., 2007). Briefly, stoichiometric amounts of each component (5 µM of TBCE, TBCB and tubulin dimer) were incubated (30℃, 30 min) in a buffer containing 0.5 M MES-NaOH, 25 mM KCl, 1 mM $MgCl_2$, 1 mM EGTA and 1 mM GTP, pH 6.7. Samples were loaded in a non-denaturing polyacrylamide gel and electrophoresis was carried out at 4℃ in a buffer containing 0.1 M MES-NaOH, 1 mM $MgCl_2$, 1 mM EGTA and 0.1 mM GTP, pH 6.7. When needed, Coomassie-stained protein bands were quantified by densitometry using QuantityOne software (Bio-Rad).

αEB and αEB–GFP complexes were formed by incubation of TBCE and TBCB or TBCB–GFP with tubulin dimers, then purified by gel filtration chromatography (Kortazar et al., 2007).

Proteolysis assays

Limited proteolysis assays of tubulin dimers were performed with distinct concentrations of subtilisin [0.5–2% (w/v)] (Fontalba et al., 1995). S-tubulin purification was based on the microtubule polymerization at 35℃ in the presence of 1 mM GTP and 2 mM $CaCl_2$, as Ca^{2+} inhibits tubulin assembly by interfering with the tubulin C-terminal residue not present in the S-tubulin monomers (Serrano et al., 1986). Polymerized microtubules were purified by ultracentrifugation (40,000 ***g***, 1 h) and subsequently depolymerized (2 h, 4℃) by adding 0.3 M KCl, followed by ultracentrifugation (12,000 ***g***, 15 min, 4℃), then loaded onto a Superdex 200 PC 3.2/30 gel filtration column equilibrated with 0.1 M MES-KOH, 1 mM $MgCl_2$, 25 mM KCl, 1 mM GTP, pH 6.7. S-tubulin fractions were pooled and concentrated by ultracentrifugation in Amicon UltraCell units. The final residue of the α-tubulin Cterminal end (Tyr; Y) was removed specifically by treating tubulin dimers with the exoprotease carboxipeptidase A (CPA). Detyrosinated tubulin (ΔYtubulin) was purified as for S-tubulin, in the absence of Ca^{2+}. Tubulin dimer dissociation activity was quantified by densitometry of tubulin dimer bands in Coomassie-stained polyacrylamide gels using QuantityOne.

Estimation of the dissociation constant of TBCE and C-terminal tail of α-tubulin by fluorescence anisotropy

The dissociation constant was estimated by fluorescence anisotropy in a Wallac Victor 2V 1420 multilabel counter (PerkinElmer). Two α-tubulin peptides N-terminally tagged with fluorescein were designed and synthesized by Genosphere Biotechnologies, with the last ten (sequence GEGEEEGEEY) or nine (sequence GEGEEEGEE) C-terminal amino acids of αtubulin separated from the fluorescein by a C6 spacer. Each peptide (0.5 nmol) was mixed with tubulin dimers (0–8 µM) in a binding buffer containing 20 mM potassium phosphate buffer, 50 mM KCl, 1 mM TCEP, pH 7.5 (30℃, 30 min). Fluorescence intensity was measured with a 485 nm excitation filter and a 535 nm emission filter. Normalized data were used to calculate the K_d (Roehrl et al., 2004).

Immunocytochemistry and confocal microscopy

HeLa cells were transiently transfected using X-tremeGENE Transfection Reagent (Roche). After 26 h, cells were fixed in 4% paraformaldehyde, permeabilized in PBS-1% Triton X-100 and stained using the B512 antibody to α-tubulin (Sigma-Aldrich) and Cy3-conjugated goat anti-mouse-IgG secondary antibody. Nuclei were stained with Hoechst 33258 fluorescent stain (Sigma-Aldrich). Images were acquired in a Zeiss Axio Observer.Z1 microscope equipped with a Yokogawa CSU-X1 Spinning Disc for live cell microscopy. In these triple-labeling experiments, images were scanned sequentially to avoid fluorescent channel emission crosstalk or bleedthrough. Images were acquired with a Photometrics QuantEM CCD camera.

Nucleotide isolation and quantification by high-pressure liquid chromatography

To analyze GTP hydrolysis during tubulin dissociation by TBCE and TBCB, we used purified tubulin dimers (0.5 nmol), which were subjected to an assembly-disassembly cycle to remove all traces of GTP, and incubated with TBCE (15 µM) and TBCB (10 µM) (30℃, 30 min) to ensure complete heterodimer dissociation. After incubation, the reaction was heated (100℃, 2 min) to separate α- and β-monomers from free nucleotides. The reaction mixture was centrifuged, loaded onto a MonoQ 5/50 column equilibrated with 20 mM HCl, and nucleotides were eluted with a linear gradient of 1 M NaCl.

Electron microscopy and 3D reconstruction

TBCE, αEB and αEB–GFP samples were negatively stained with 2% (w/v) uranyl acetate and imaged in a JEM 1200 EX-II transmission electron microscope (JEOL) operated at 100 kV under low-dose conditions. Micrographs were recorded on Kodak SO-163 plates at 60,000 magnification, digitized using a Photoscan TD (Zeiss) and CTF-corrected with CTFfind3 and XMIPP (Marabini et al., 1996; Mindell and Grigorieff, 2003; Scheres et al., 2008). A total of 12,000 particles were selected for TBCE, 26,129 for αEB, and 16,702 for αEB–GFP samples, and were downsampled to 4.66 Å/pixel and normalized using XMIPP procedures. All particles were initially classified using clustering reference-free methods implemented in XMIPP (Marabini et al., 1996; Sorzano et al., 2010). Angular refinement was performed using EMAN and XMIPP (Marabini et al., 1996; Ludtke et al., 1999; Scheres et al., 2008). Resolution was estimated by Fourier shell correlation (FSC) at 0.3 criteria (Penczek, 2002). The atomic structures were fitted manually into the EM density maps using UCSF Chimera (Pettersen et al., 2004). The final docking solutions for TBCE and the αEB complex were obtained by fulfilling the constraints imposed by the biochemical data for the protein–protein interactions of the complex components and by the structural requirements of the 3D reconstructions. Goodness of docking was quantified using Chimera software, based on the correlation between the models built for TBCE and the αEB complex and their 3D reconstructions, which showed values of 0.76 and 0.78, respectively.

Crystallization and structure determination of human TBCEubl

Sitting drops were prepared by mixing 0.1 µl protein (25 mg/ml) with the same volume of reservoir solution. Two crystal forms of the TBCEubl protein were obtained. The A form was obtained from 100 mM Tris-HCl pH 8.5, 200 mM sodium acetate and 30% (v/w) PEG 4000, and the B form from 100 mM Bis-Tris pH 6.5, 45% (v/v) PEG 400 and 100 mM praseodymium (III) acetate. Diffraction data for both crystal forms were collected on the micro-focus beamline ID23-2 (ESRF, Grenoble, France) using a CCD detector (MarMosaic 225) with a 0.8726 Å wavelength and 10-µm beam diameter. Both data sets were indexed and integrated using XDS (Kabsch, 2010) and scaled with SCALA (Steller et al., 1997). Intensities were converted into structure-factor amplitudes using TRUNCATE (French and Wilson, 1978; CCP4, 1994). The structure of the crystal form B was solved by the SAD protocol of Auto-Rickshaw (Panjikar et al., 2005; Panjikar et al., 2009) and used to solve the structure of the crystal form A by molecular replacement using the PHASER program (McCoy et al., 2007). Both crystal forms were further refined in REFMAC5 (Murshudov et al., 1997) using the maximum-likelihood target function and including TLS parameters (Winn et al., 2001).

Acknowledgements

We thank the staff of ID29 Beamline at the ESRF (Grenoble) and the Automated Crystallography Platform at PCB (Barcelona). We acknowledge G. Montoya (Copenhagen University) for his help with the fluorescence polarization experiments, P. Berger (Paul Scherrer Institute, Switzerland) for providing the pSI-DAL2 plasmid and N. Cowan (New York University Medical Center, NY) for his gift of Human TBCE cDNA. We thank C. Mark for editorial assistance.

Competing interests

The authors declare no competing or financial interests.

Author contributions

M.S., G.C., A.C., J.M.B., R.J. and A.C. performed experiments. M.S., G.C., M.C., J.M.B., J.C.Z. and J.M.V. designed the experiments. M.S., M.C., J.M.B., J.C.Z. and J.M.V. wrote the manuscript.

Funding

This work was supported by the Spanish Ministry of Science and Innovation [grant numbers CONSOLIDER CSD 2006-23 to M.C., J.C.Z. and J.M.V., BFU2011-22588 to M.C., BFU2011-25090 to J.M.B., BFU2013-44202 to J.M.V., and

BFU2010-18948 to J.C.Z.]; the Madrid Regional Government [grant number S2013/MIT-2807 to J.M.V.]; the Generalitat de Catalunya [grant number SGR2009-1309 to M.C.]; the Instituto de Investigación Marqués de Valdecilla (IDIVAL); the Universidad de Cantabria [grant number 02.VP01.64005 to J.C.Z.]; and the European Commission FP7 Cooperation Project SILVER - GA [grant number 260644 to M.C.].

Supplementary material

Supplementary material available online at
http://jcs.biologists.org/lookup/suppl/doi:10.1242/jcs.167387/-/DC1

References

Alushin, G. M., Lander, G. C., Kellogg, E. H., Zhang, R., Baker, D. and Nogales, E. (2014). High-resolution microtubule structures reveal the structural transitions in αβ-tubulin upon GTP hydrolysis. *Cell* **157**, 1117-1129.

Avila, J., Soares, H., Fanarraga, M. L. and Zabala, J. C. (2008). Isolation of microtubules and microtubule proteins. *Curr. Protoc. Cell Biol.* **39**, 3.29.1-3.29.28.

Bartolini, F., Tian, G., Piehl, M., Cassimeris, L., Lewis, S. A. and Cowan, N. J. (2005). Identification of a novel tubulin-destabilizing protein related to the chaperone cofactor E. *J. Cell Sci.* **118**, 1197-1207.

Campo, R., Fontalba, A., Sanchez, L. M. and Zabala, J. C. (1994). A 14 kDa release factor is involved in GTP-dependent beta-tubulin folding. *FEBS Lett.* **353**, 162-166.

Caplow, M. and Fee, L. (2002). Dissociation of the tubulin dimer is extremely slow, thermodynamically very unfavorable, and reversible in the absence of an energy source. *Mol. Biol. Cell* **13**, 2120-2131.

Carranza, G., Castaño, R., Fanarraga, M. L., Villegas, J. C., Gonçalves, J., Soares, H., Avila, J., Marenchino, M., Campos-Olivas, R., Montoya, G. et al. (2013). Autoinhibition of TBCB regulates EB1-mediated microtubule dynamics. *Cell. Mol. Life Sci.* **70**, 357-371.

Collaborative Computational Project, Number 4 (CCP4) (1994). The CCP4 suite: programs for protein crystallography. *Acta Crystallogr. D Biol. Crystallogr.* **50**, 760-763.

Cook, W. J., Jeffrey, L. C., Kasperek, E. and Pickart, C. M. (1994). Structure of tetraubiquitin shows how multiubiquitin chains can be formed. *J. Mol. Biol.* **236**, 601-609.

Fontalba, A., Paciucci, R., Avila, J. and Zabala, J. C. (1993). Incorporation of tubulin subunits into dimers requires GTP hydrolysis. *J. Cell Sci.* **106**, 627-632.

Fontalba, A., Avila, J. and Zabala, J. C. (1995). Beta-tubulin folding is modulated by the isotype-specific carboxy-terminal domain. *J. Mol. Biol.* **246**, 628-636.

French, G. S. and Wilson, K. S. (1978). On the treatment of negative intensity observations. *Acta Crystallogr. A* **34**, 517-525.

Grynberg, M., Jaroszewski, L. and Godzik, A. (2003). Domain analysis of the tubulin cofactor system: a model for tubulin folding and dimerization. *BMC Bioinformatics* **4**, 46.

Hothorn, M., Belkhadir, Y., Dreux, M., Dabi, T., Noel, J. P., Wilson, I. A. and Chory, J. (2011). Structural basis of steroid hormone perception by the receptor kinase BRI1. *Nature* **474**, 467-471.

Jacobs, M. (1975). Tubulin nucleotide reactions and their role in microtubule assembly and dissociation. *Ann. N. Y. Acad. Sci.* **253**, 562-572.

Kabsch, W. (2010). XDS. *Acta Crystallogr. D Biol. Crystallogr.* **66**, 125-132.

Kaplun, L., Tzirkin, R., Bakhrat, A., Shabek, N., Ivantsiv, Y. and Raveh, D. (2005). The DNA damage-inducible UbL-UbA protein Ddi1 participates in Mec1-mediated degradation of Ho endonuclease. *Mol. Cell. Biol.* **25**, 5355-5362.

Kaverina, I. and Straube, A. (2011). Regulation of cell migration by dynamic microtubules. *Semin. Cell Dev. Biol.* **22**, 968-974.

Keller, C. E. and Lauring, B. P. (2005). Possible regulation of microtubules through destabilization of tubulin. *Trends Cell Biol.* **15**, 571-573.

Kortazar, D., Carranza, G., Bellido, J., Villegas, J. C., Fanarraga, M. L. and Zabala, J. C. (2006). Native tubulin-folding cofactor E purified from baculovirus-infected Sf9 cells dissociates tubulin dimers. *Protein Expr. Purif.* **49**, 196-202.

Kortazar, D., Fanarraga, M. L., Carranza, G., Bellido, J., Villegas, J. C., Ávila, J. and Zabala, J. C. (2007). Role of cofactors B (TBCB) and E (TBCE) in tubulin heterodimer dissociation. *Exp. Cell Res.* **313**, 425-436.

Lopez-Fanarraga, M., Avila, J., Guasch, A., Coll, M. and Zabala, J. C. (2001). Review: postchaperonin tubulin folding cofactors and their role in microtubule dynamics. *J. Struct. Biol.* **135**, 219-229.

Ludtke, S. J., Baldwin, P. R. and Chiu, W. (1999). EMAN: semiautomated software for high-resolution single-particle reconstructions. *J. Struct. Biol.* **128**, 82-97.

Lundin, V. F., Leroux, M. R. and Stirling, P. C. (2010). Quality control of cytoskeletal proteins and human disease. *Trends Biochem. Sci.* **35**, 288-297.

Lytle, B. L., Peterson, F. C., Qiu, S. H., Luo, M., Zhao, Q., Markley, J. L. and Volkman, B. F. (2004). Solution structure of a ubiquitin-like domain from tubulin-binding cofactor B. *J. Biol. Chem.* **279**, 46787-46793.

Marabini, R., Masegosa, I. M., San Martin, M. C., Marco, S., Fernández, J. J., de la Fraga, L. G., Vaquerizo, C. and Carazo, J. M. (1996). Xmipp: an image processing package for electron microscopy. *J. Struct. Biol.* **116**, 237-240.

Martín, L., Fanarraga, M. L., Aloria, K. and Zabala, J. C. (2000). Tubulin folding cofactor D is a microtubule destabilizing protein. *FEBS Lett.* **470**, 93-95.

McCoy, A. J., Grosse-Kunstleve, R. W., Adams, P. D., Winn, M. D., Storoni, L. C. and Read, R. J. (2007). Phaser crystallographic software. *J. Appl. Crystallogr.* **40**, 658-674.

Mi, L., Gan, N., Cheema, A., Dakshanamurthy, S., Wang, X., Yang, D. C. H. and Chung, F. L. (2009). Cancer preventive isothiocyanates induce selective degradation of cellular α- and β-Tubulins by proteasomes. *J. Biol. Chem.* **284**, 17039-17051.

Mindell, J. A. and Grigorieff, N. (2003). Accurate determination of local defocus and specimen tilt in electron microscopy. *J. Struct. Biol.* **142**, 334-347.

Mitchison, T. and Kirschner, M. (1984). Dynamic instability of microtubule growth. *Nature* **312**, 237-242.

Murshudov, G. N., Vagin, A. A. and Dodson, E. J. (1997). Refinement of macromolecular structures by the maximum-likelihood method. *Acta Crystallogr. D Biol. Crystallogr.* **53**, 240-255.

Nogales, E., Wolf, S. G. and Downing, K. H. (1998). Structure of the alpha beta tubulin dimer by electron crystallography. *Nature* **391**, 199-203.

Panjikar, S., Parthasarathy, V., Lamzin, V. S., Weiss, M. S. and Tucker, P. A. (2005). Auto-rickshaw: an automated crystal structure determination platform as an efficient tool for the validation of an X-ray diffraction experiment. *Acta Crystallogr. D Biol. Crystallogr.* **61**, 449-457.

Panjikar, S., Parthasarathy, V., Lamzin, V. S., Weiss, M. S. and Tucker, P. A. (2009). On the combination of molecular replacement and single-wavelength anomalous diffraction phasing for automated structure determination. *Acta Crystallogr. D Biol. Crystallogr.* **65**, 1089-1097.

Penczek, P. A. (2002). Three-dimensional spectral signal-to-noise ratio for a class of reconstruction algorithms. *J. Struct. Biol.* **138**, 34-46.

Pettersen, E. F., Goddard, T. D., Huang, C. C., Couch, G. S., Greenblatt, D. M., Meng, E. C. and Ferrin, T. E. (2004). UCSF Chimera – a visualization system for exploratory research and analysis. *J. Comput. Chem.* **25**, 1605-1612.

Riedinger, C., Boehringer, J., Trempe, J. F., Lowe, E. D., Brown, N. R., Gehring, K., Noble, M. E., Gordon, C. and Endicott, J. A. (2010). Structure of Rpn10 and its interactions with polyubiquitin chains and the proteasome subunit Rpn12. *J. Biol. Chem.* **285**, 33992-34003.

Roehrl, M. H., Wang, J. Y. and Wagner, G. (2004). A general framework for development and data analysis of competitive high-throughput screens for small-molecule inhibitors of protein-protein interactions by fluorescence polarization. *Biochemistry* **43**, 16056-16066.

Scheres, S. H., Núñez-Ramírez, R., Sorzano, C. O., Carazo, J. M. and Marabini, R. (2008). Image processing for electron microscopy single-particle analysis using XMIPP. *Nat. Protoc.* **3**, 977-990.

Serrano, L., de la Torre, J., Luduena, R. F. and Avila, J. (1986). The removal of the carboxy-terminal region of tubulin favors its vinblastine-induced aggregation into spiral-like structures. *Arch. Biochem. Biophys.* **249**, 611-615.

Sorzano, C. O., Bilbao-Castro, J. R., Shkolnisky, Y., Alcorlo, M., Melero, R., Caffarena-Fernández, G., Li, M., Xu, G., Marabini, R. and Carazo, J. M. (2010). A clustering approach to multireference alignment of single-particle projections in electron microscopy. *J. Struct. Biol.* **171**, 197-206.

Steinmetz, M. O. and Akhmanova, A. (2008). Capturing protein tails by CAP-Gly domains. *Trends Biochem. Sci.* **33**, 535-545.

Steller, I., Bolotovsky, R. and Rossmann, M. G. (1997). An algorithm for automatic indexing of oscillation images using Fourier analysis. *J. Appl. Crystallogr.* **30**, 1036-1040.

Tian, G., Huang, Y., Rommelaere, H., Vandekerckhove, J., Ampe, C. and Cowan, N. J. (1996). Pathway leading to correctly folded beta-tubulin. *Cell* **86**, 287-296.

Tian, G., Lewis, S. A., Feierbach, B., Stearns, T., Rommelaere, H., Ampe, C. and Cowan, N. J. (1997). Tubulin subunits exist in an activated conformational state generated and maintained by protein cofactors. *J. Cell Biol.* **138**, 821-832.

Tian, G., Bhamidipati, A., Cowan, N. J. and Lewis, S. A. (1999). Tubulin folding cofactors as GTPase-activating proteins. GTP hydrolysis and the assembly of the alpha/beta-tubulin heterodimer. *J. Biol. Chem.* **274**, 24054-24058.

Upadhya, S. C. and Hegde, A. N. (2003). A potential proteasome-interacting motif within the ubiquitin-like domain of parkin and other proteins. *Trends Biochem. Sci.* **28**, 280-283.

Verhey, K. J. and Gaertig, J. (2007). The tubulin code. *Cell Cycle* **6**, 2152-2160.

Voloshin, O., Gocheva, Y., Gutnick, M., Movshovich, N., Bakhrat, A., Baranes-Bachar, K., Bar-Zvi, D., Parvari, R., Gheber, L. and Raveh, D. (2010). Tubulin chaperone E binds microtubules and proteasomes and protects against misfolded protein stress. *Cell. Mol. Life Sci.* **67**, 2025-2038.

Winn, M. D., Isupov, M. N. and Murshudov, G. N. (2001). Use of TLS parameters to model anisotropic displacements in macromolecular refinement. *Acta Crystallogr. D Biol. Crystallogr.* **57**, 122-133.

Zabala, J. C. and Cowan, N. J. (1992). Tubulin dimer formation via the release of alpha- and beta-tubulin monomers from multimolecular complexes. *Cell Motil. Cytoskeleton* **23**, 222-230.

SUPPLEMENTAL INFORMATION

The structure of the TBCE/TBCB chaperones and α-tubulin complex shows a tubulin dimer dissociation mechanism

Marina Serna, Gerardo Carranza, Jaime Martín-Benito, Robert Janowski, Albert Canals, Miquel Coll, Juan Carlos Zabala, José María Valpuesta

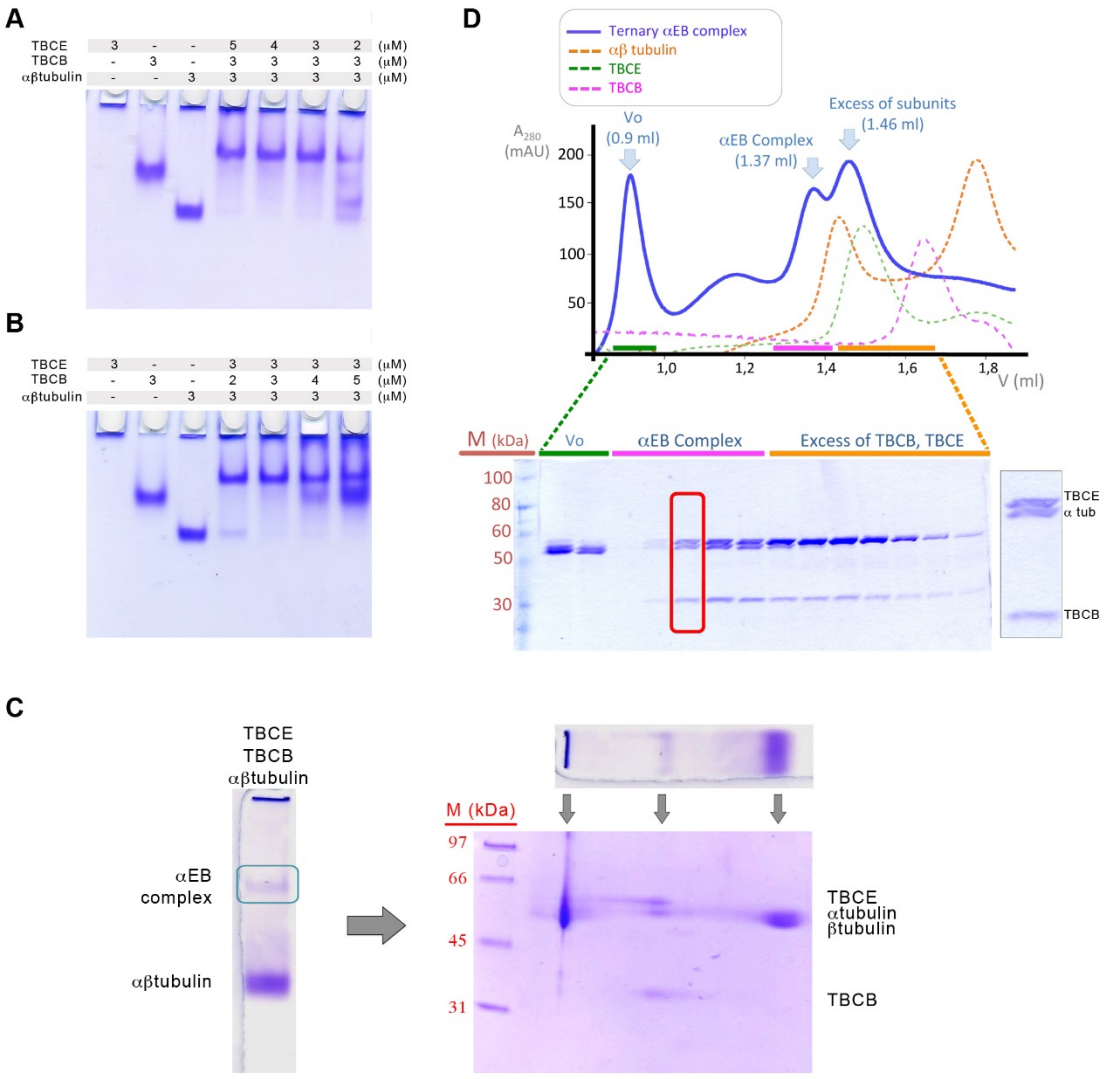

Fig. S1. Tubulin dimer dissociation assay and purification. **(A, B)** Coomassie-stained native polyacrylamide gel showing the ability of TBCE (A) and TBCB (B) to dissociate tubulin dimers, evaluated as decreasing intensity of the tubulin dimer band. Various chaperone concentrations were tested to confirm that stoichiometric amounts of these cofactors were sufficient to dissociate the tubulin dimers completely. **(C)** 2D native/SDS-PAGE was performed (see Carranza et al., 2013). Left, TBCB and TBCE and tubulin heterodimers were incubated (30°C, 30 min) and loaded onto a 6% native gel. Right, after electrophoresis, bands were excised and samples loaded onto an SDS gel. The presence of TBCE, TBCB and α-tubulin was confirmed by western blot using specific antibodies. An excess of tubulin dimers was used to illustrate the presence of α and β tubulin monomers in the dimer band. **(D)** Isolation of the ternary complex formed by TBCB, TBCE and α-tubulin. The elution profiles of TBCB, TBCE, αβ-tubulin and αEB complex formation were analyzed by gel filtration on a Superdex 200 PC 3.2/30 column (GE-Healthcare), followed by SDS-PAGE (bottom).

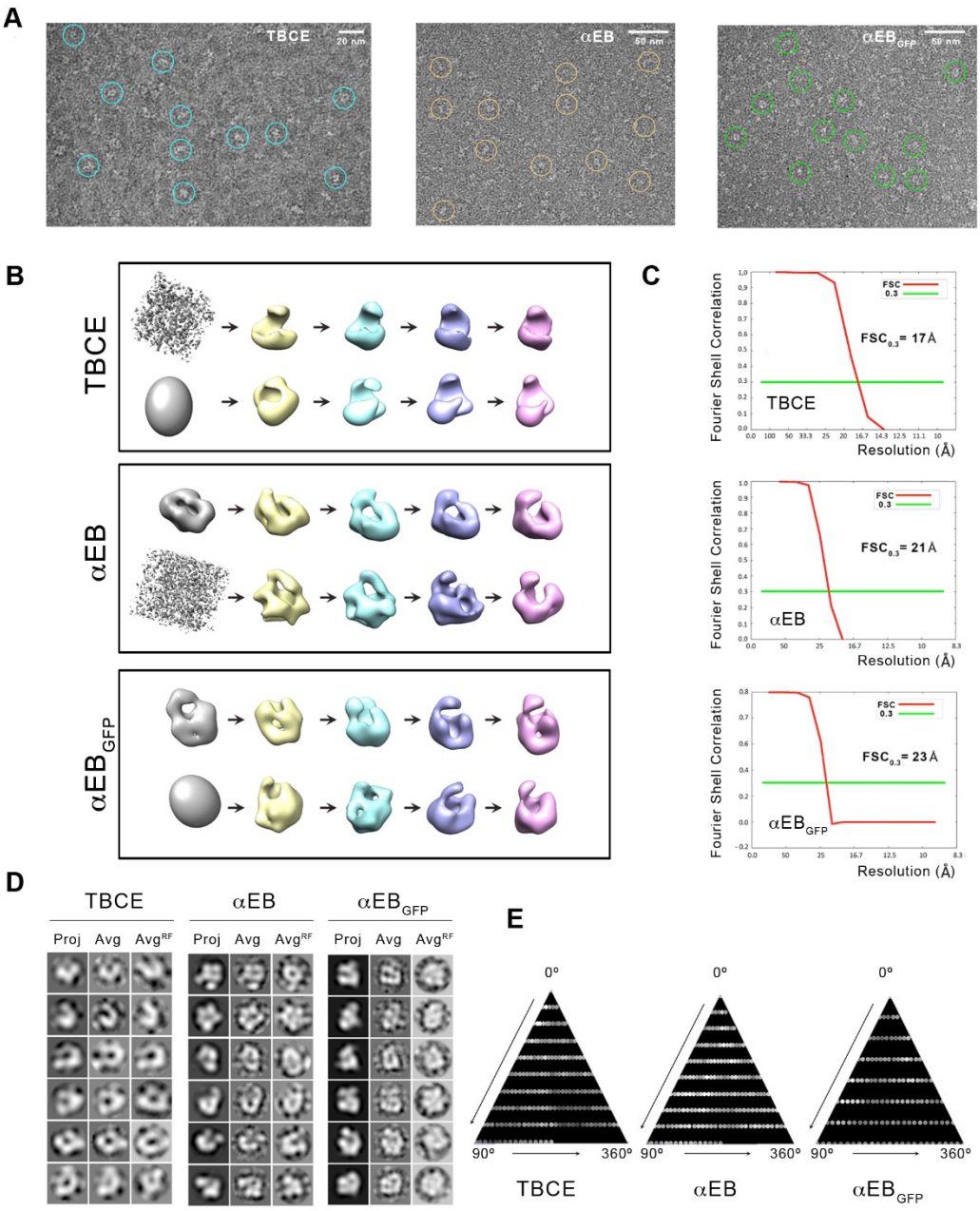

Figure S2. 3D reconstruction of TBCE, αEB and αEB$_{GFP}$ complexes. **(A)** Representative area of micrographs from TBCE (left), αEB (center) and αEB$_{GFP}$ samples (right). **(B)** Examples of volume evolution during iterative refinement using different initial references. Convergence was achieved in all cases. **(C)** Fourier shell correlation curves of 3D reconstructions of TBCE, αEB and αEB$_{GFP}$ showing the final resolutions of 18, 21 and 24 Å, respectively (0.3 criterion). **(D)** Representative projections (Proj) of the final reconstruction of each sample are shown next to the associated class averages (Avg) and the average obtained after the initial reference-free classification (Avg^{RF}). The similarity among these images strengthens the quality of the reconstructions. **(E)** Diagram showing the distribution of projection orientation used during refinement. Brighter dots indicate a larger number of particles.

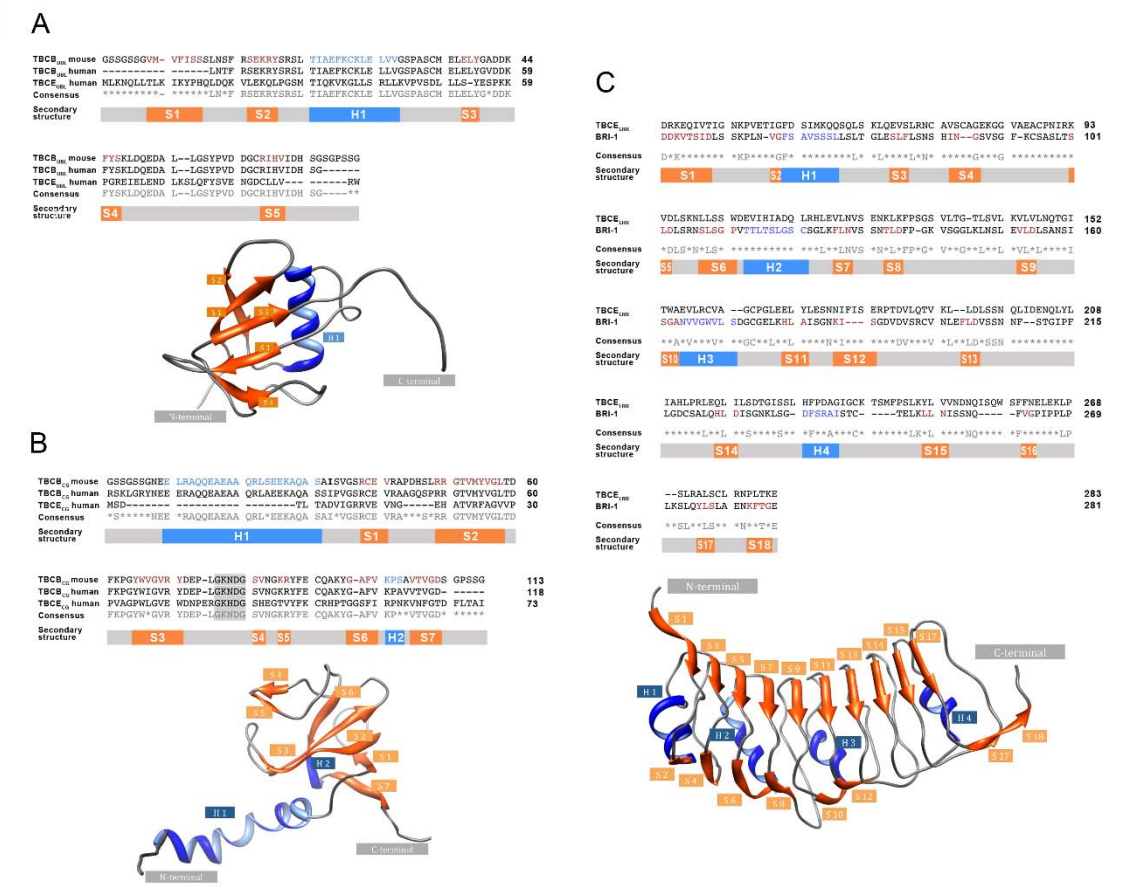

Fig. S3. Atomic structures of the domains used for docking into the 3D reconstructions of TBCE and the αEB complex. **(A)** Top, sequence alignment of the UBL domains of murine TBCB, human TBCB and human TBCE. In the first sequence, β-strand and α-helix residues of the atomic structure of murine UBL (PDB 1V6E) are in orange and blue, respectively. The secondary elements of the atomic structure of murine TBCB UBL domain are shown, with β-strands numbered S1-S5 in orange and the single α-helix in blue. Bottom, atomic structure of the UBL domain of murine TBCB with color and number codes as above for the secondary structure elements. **(B)** Top, sequence alignment of CAP-Gly domains of murine TBCB, human TBCB and human TBCE. The secondary elements of murine TBCB CAP-Gly domain (PDB 1WHG) are shown beneath the sequences. Bottom, atomic structure of murine the CAP-Gly domain with color and number codes as above for the secondary structure elements. **(C)** Amino acid sequence alignment of TBCE LRR domain and the homologous domain in the BRI1 kinase. The secondary structure elements of the last domain are shown beneath the sequence alignment and in the LRR structure of the BRI-1 protein (PDB 3RJ0).

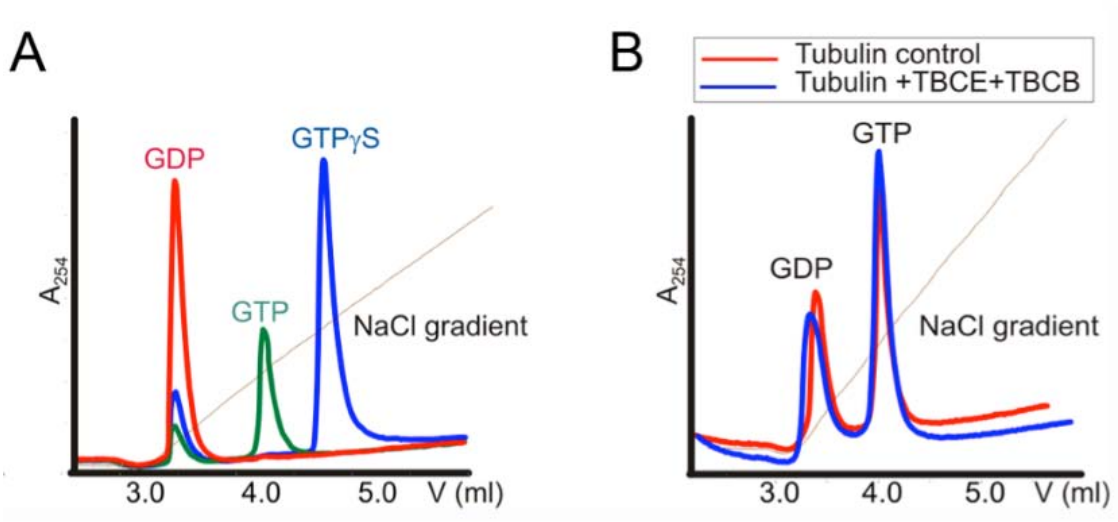

Fig. S4. Tubulin dimer dissociation does not require GTP hydrolysis. (A) Isolation of GTP, GDP and GTPγS on a high-resolution Mono Q 5/50 anion exchange column. **(B)** Detection of tubulin-bound nucleotides (GTP or GDP). Control tubulin (red) and dissociated tubulin in the presence of tubulin cofactors (blue).

Movie 1. Molecular architecture of the complex formed by α-tubulin and the molecular chaperones TBCE and the TBC (αEB complex).
The movie shows the 3D reconstruction of the αEB complex and the docking of the atomic structures of the different domains of the three proteins, using also the biochemical information supporting this molecular architecture. Finally, the movie shows the proposed model for the dissociation of tubulin dimers by the EB complex and its possible effect in tubulin degradation.

Download Table S1

Download Table S2